Electronic Supplementary Material (ESI) for Catalysis Science & Technology.
This journal is © The Royal Society of Chemistry 2014

Supporting information

Long-term, Stable, and Improved Oxygen-Reduction Performance of Titania-supported PtPb Nanoparticles

Takao Gunji, Govindachetty Saravanan, Toyokazu Tanabe, Takashi Tsuda, Masahiro Miyauchi, Genki Kobayashi, Hideki Abe, and Futoshi Matsumoto

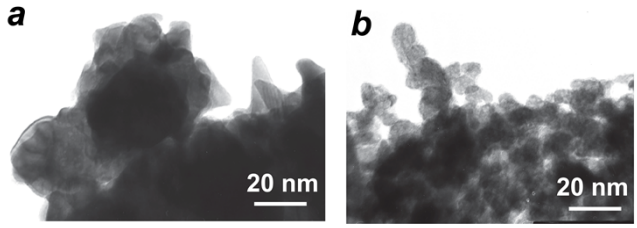

Figure S1. Bright-field TEM images of the Pt (*a*) and PtPb NPs (*b*).

Figure S1 represents the bright-field TEM images of the Pt and PtPb nanoparticles (NPs). The NPs were agglomerated and formed as large-sized clusters for the both Pt and PtPb NPs.

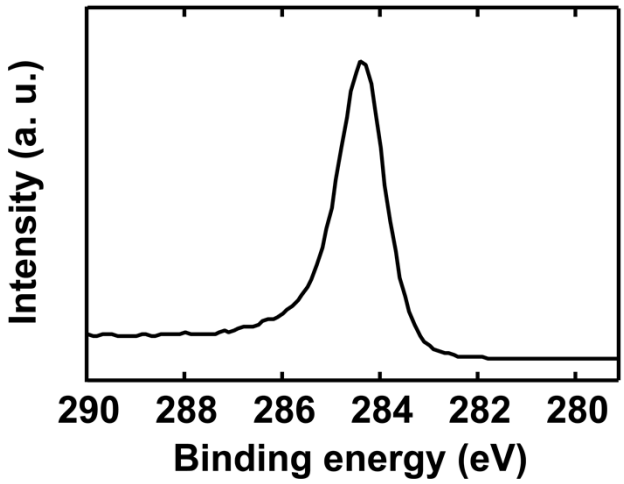

Figure S2. X-ray photoelectron spectral profile for PtPb/TiO_2 in the region of C 1*s*.

The XPS spectral profile of C 1*s* region for PtPb/TiO_2 showed the binding energy at 284.4 eV (Figure S2) indicating that the XPS measurements were free from charging effect.

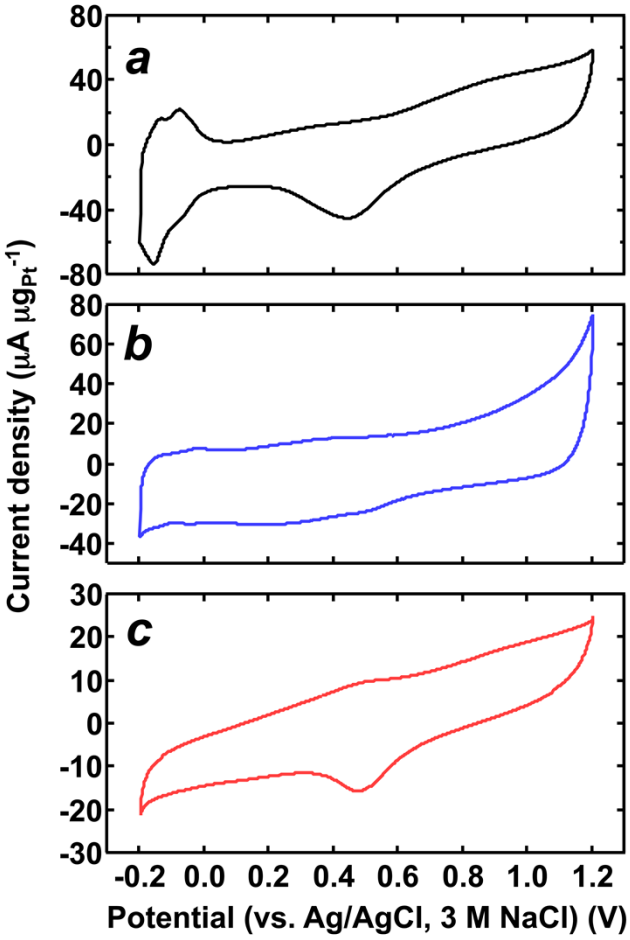

Figure S3. Cyclic voltammograms of the Pt/VC (*a*), Pt/TiO_2 (*b*), and PtPb/TiO_2 (*c*) coated electrodes in Ar-saturated aqueous 0.1 M H_2SO_4 solution at a scan rate of 50 mVs^{-1}.

Figure S3*a* shows the characteristic CV of the commercially available Pt/VC (Pt loading: 20 wt.%) in Ar-saturated aqueous 0.1 M H_2SO_4 solution. The characteristic both hydrogen adsorption and desorption peaks on the Pt surface were observed in the regions of -0.2 to 0.1 V. Also, the characteristic peak for the formation of oxide moieties (0.5 to 1.2 V) in the anodic scan and their corresponding reduction (0.2 to 0.8 V) in the cathodic scan on the Pt surface was observed. Pt/TiO_2 also showed the similar trend, however, the weak peaks for hydrogen adsorption and desorption (-0.2 to 0.1 V) as well as the peak for the formation of oxide moieties (0.08 to 0.7 V) and their corresponding reduction peak (0.06 to 0.75 V) were observed (Figure S3*b*). Whereas, no such characteristic hydrogen adsorption and desorption peaks were observed for PtPb/TiO_2, however, the peak for the formation of oxide moieties (0.2 to 0.65 V) and their corresponding reduction (0.3 to 0.7 V) were observed solely on PtPb/TiO_2 (Figure S3*c*). It

should be noted that the electric potential region for the formation of oxide moieties for both Pt/TiO_2 and $PtPb/TiO_2$ in the anodic scan is shifted to a lower electric potential region compared to the commercially available Pt/VC, indicating that water in the supporting electrolyte of H_2SO_4 can be oxidized at a relatively lower electric potential during the anodic scan when the Pt or PtPb NPs were dispersed on the TiO_2 support. Therefore, the nature of the support, composition of the NPs as well as their interactions with the support, and the electronic structure of the NPs are most likely influenced the observed electrochemical behavior.

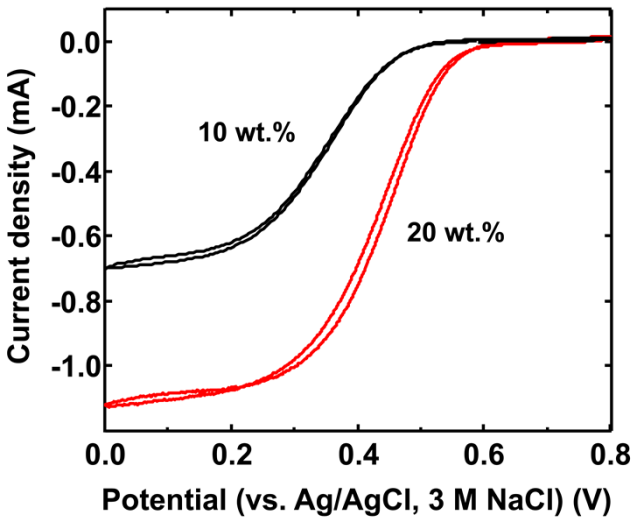

Figure S4. Cyclic voltammograms of commercially available Pt/VC having the loading weight of 10 wt.% and 20 wt.% on a GC electrode in O_2-saturated aqueous 0.1 M H_2SO_4 solution at a scan rate of 10 mVs^{-1}.

Figure S4 shows the characteristic CVs of the commercially available Pt/VC coated GC electrode in O_2-satuarated aqueous 0.1 M H_2SO_4 solution. The onset potential of the commercially available Pt/VC coated GC electrode having the loading weight of 10 wt.% and 20 wt.% showed at ~ 0.5 and ~ 0.6 V, respectively, indicating that the onset potential is strongly depended on the loading weight of Pt on the electrode.

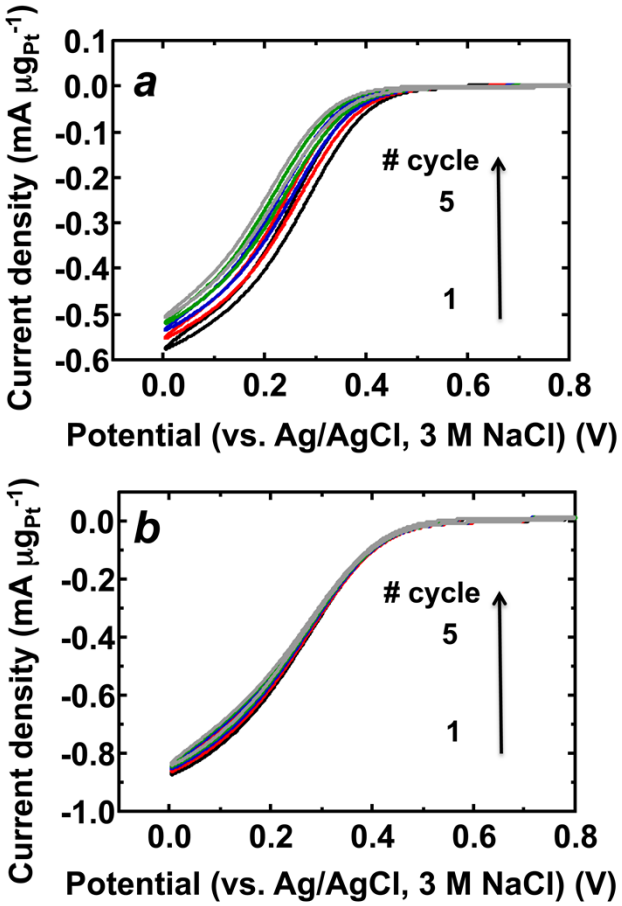

Figure S5. ORR performance of Pt/VC (*a*) and PtPb/TiO_2 (*b*) after 500 electric cycles in O_2-saturated 0.1 M H_2SO_4 solution at a scan rate of 50 mVs^{-1}.

Figure S5 shows the ORR performance of Pt/VC and PtPb/TiO_2, which are cycled under electric potential in the presence of Ar-saturated 0.1 M H_2SO_4 aqueous solution between the potential region of -0.2 and 1.2 V for 500 electric cycles. Both the onset potential (0.56 V) and the mass activity (0.40 mA μg_{Pt}^{-1} at 0.2 V) of Pt/VC were steadily decreased with increasing of the ORR cycles. Whereas, PtPb/TiO_2 didn`t show any significant changes in both the onset potential (0.61 V) and the mass activity (0.58 mA μg_{Pt}^{-1} at 0.2 V), indicating that PtPb/TiO_2 possesses the stable and the long-term electrocatalytic ORR performance even after 500 electric potential cycling.

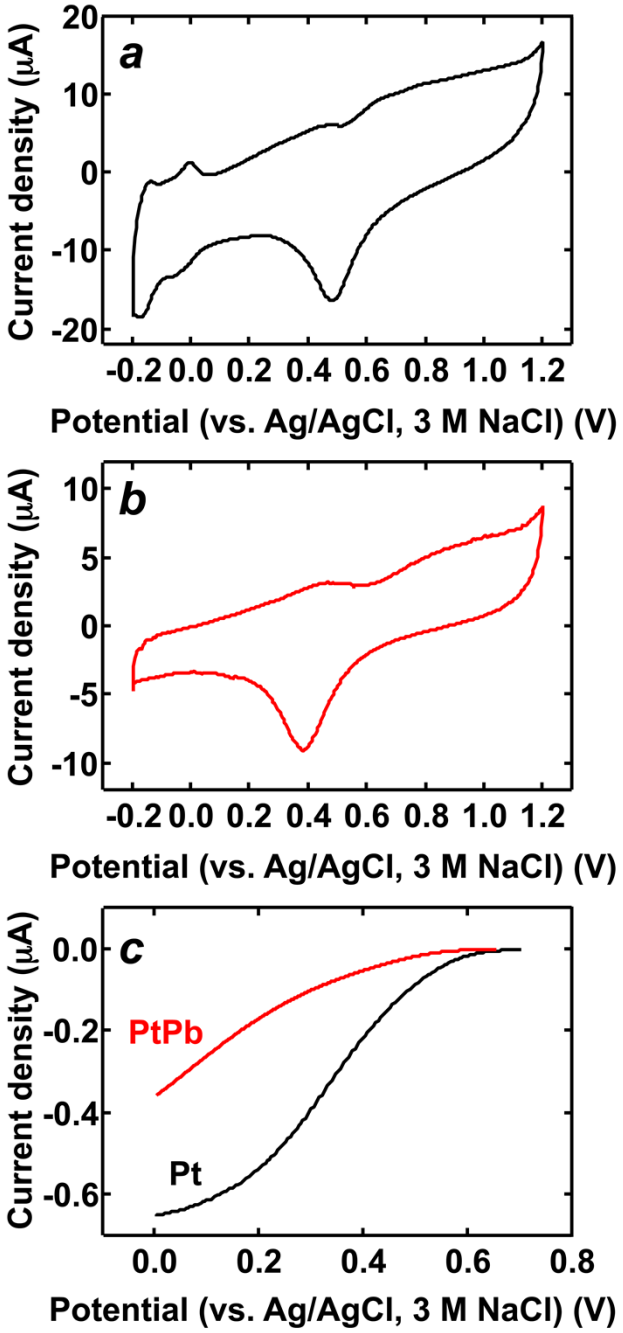

Figure S6. Cyclic voltammograms of Pt NPs (*a*) and PtPb NPs (*b*) on a GC electrode in Ar-saturated aqueous 0.1 M H_2SO_4 solution at a scan rate of 50 mVs^{-1}. (c) The cathodic potential sweeps for the Pt and PtPb NPs on a GC electrode in O_2-saturated 0.1 M H_2SO_4 solution at a scan rate of 10 mVs^{-1} and at a rotation rate of 2000 rpm.

Figure S6*a* shows the characteristic CVs of the Pt NPs on a GC electrode in Ar-saturated aqueous 0.1 M H_2SO_4 solution. The characteristic both hydrogen adsorption and desorption peaks on the Pt surface were observed in the regions of -0.2 to 0.1 V. Also, the characteristic peak for the formation of oxide moieties (0.5 to 1.2 V) in anodic scan and their corresponding reduction (0.2 to 0.8 V) in cathodic scan on the Pt surface was observed. Whereas, no such characteristic hydrogen adsorption and desorption peaks were observed for the PtPb NPs on the GC electrode, however, the peak for the formation of oxide moieties (0.2 to 0.65 V) and their corresponding reduction (0.1 to 0.7 V) were observed solely on the PtPb NPs on the GC electrode (Figure S6*b*). Therefore, the electronic structure of catalytic sites are most likely influenced the observed electrochemical behavior.

The ORR performance of support-free PtPb and Pt NPs were examined to investigate the influence of the TiO_2 support towards ORR. The ORR activity of support-free PtPb decreased steeply compared to the Pt NPs in terms of the onset potential and the ORR current density (Figure S6*c*). The PtPb NPs showed the ORR activity having the onset potential and the ORR current density measured at 0.2 V is 0.52 V and 0.16 mA, respectively. The Pt NPs also showed the ORR activity, however, having the substantially higher ORR activity compared to the PtPb NPs. The ORR current density of the Pt NPs was measured at 0.2 V is 0.53 mA μg_{Pt}^{-1}. In addition, the onset potential of the Pt NPs is shifted by 120 mV and observed at 0.64 V compared to the PtPb NPs. The inferior activity of the PtPb NPs compared to the Pt NPs indicates that the PtPb NPs can`t be solely utilized as cathode catalyst for ORR.

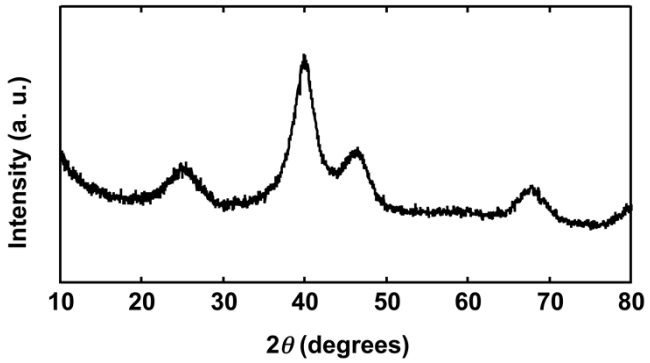

Figure S7. *p*XRD profile for the commercially available Pt/VC (20 wt. %)

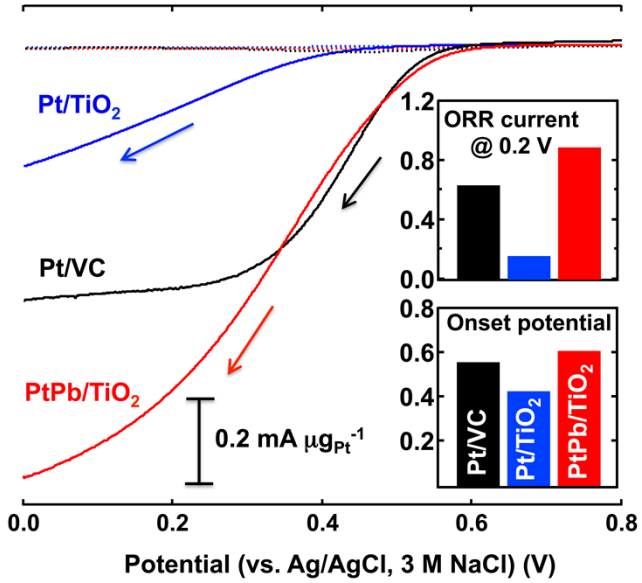

Figure S8. The cathodic potential sweeps (solid lines) for Pt/VC, Pt/TiO_2, and PtPb/TiO_2 in O_2-saturated 0.1 M H_2SO_4 solution at a scan rate of 10 mVs^{-1} and at a rotation rate of 2000 rpm. The blank cathodic potential sweeps of these electrodes are shown as dotted lines. The insets show the ORR current measured at 0.2 V and the onset potential for Pt/VC (black), Pt/TiO_2 (blue), and PtPb/TiO_2 (red).

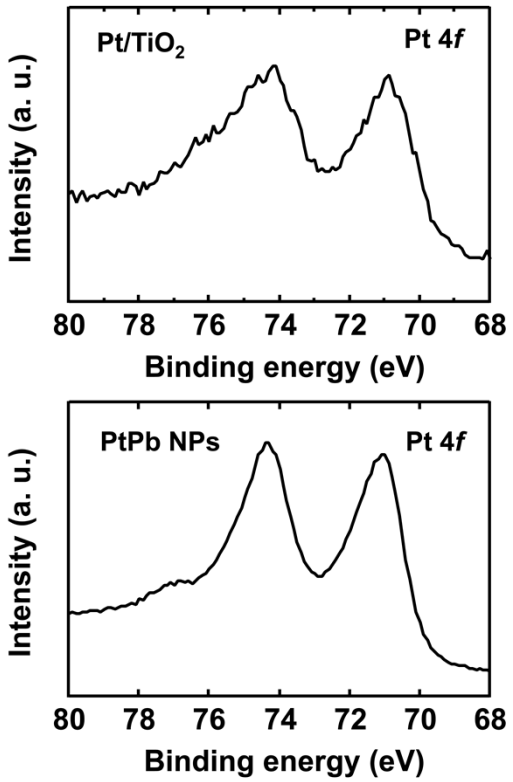

Figure S9. X-ray photoelectron spectral profiles for Pt/TiO_2 and PtPb NPs in the region of Pt 4*f*.

ICP-MS analysis

Samples	Pt loading weight (Wt. %)	CPS	Concentration (ppb)
Pt/VC	20	563041.3733	72.542596
Pt/TiO_2	5.32	825122.22	106.3295236
$PtPb/TiO_2$	2.34	363721.1067	46.84663426

ICP-MS analysis over the catalysts were performed to evaluate the Pt-loading weight in the catalysts. The Pt-loading weight of the catalysts was utilized to evaluate the ORR mass activity. The loading weight of Pt on the Pt/VC, Pt/TiO_2, and $PtPb/TiO_2$ electrode was estimated to be 1.74, 1.53, and 0.67 μg, respectively.